

Preparation of Three-Dimensional Porous Graphene by Hydrothermal and Chemical Reduction with Ascorbic Acid and its Electrochemical Properties

Hui Liu, Baiqing Sun, Peiyuan Zhu, Chenyu Liu, Gaimei Zhang,* Dongdong Wang, Xiaoli Song, Jiazi Shi, Yonggang Yang, and Jiandong Lu^[a]

Three-dimensional porous graphene (3D-PG) has attracted much attention due to its excellent electrochemical performance. Chemical reduction is one of common methods for preparing porous graphene. In order to develop a green and facile method for preparing three-dimensional porous graphene, in this paper, 3D-PG was fabricated by reduction of graphene oxide (GO) with ascorbic acid (AA) as reductant in hydrothermal condition based on non-toxic, non-flammable and mild reducing performance of ascorbic acid. It was found that the size and distribution of pores could be controlled by

the reduction time and the concentration of AA in the solution. The pore sizes in R0, R1 and R2 were in the range of 0.5–1 μm , 1–1.5 μm , and 1.5–3 μm , respectively. It was found that the average pore size and volume increased along with the amount of reductants. Under optimal conditions – a reaction time of 20 h and a ratio of GO to AA = 1:1 – the CV area of the so-obtained sample R1-20 at 100 mV was 0.06 and the specific capacitance of the 3D-PG electrode reaches 153.5 $\text{F}\cdot\text{g}^{-1}$, which is suitable for use in supercapacitors.

Introduction

Graphene can be applied in batteries as an electrode material and in composites owing to its high carrier mobility, good conductivity,^[1] high power density, high thermal conductivity,^[2] excellent chemical stability and electrochemical characteristics.^[3] However, graphene is easy to agglomerate and stack due to van der Waals forces, which leads to the decrease in specific surface area and even of the specific capacitance of the prepared electrode material.^[4] Three-dimensional porous graphene (3D-PG) composed of two-dimensional graphene has a three-dimensional network structure and can reduce the agglomeration of graphene,^[5] which exhibits a great specific surface, excellent mechanical strength,^[6] ultra-high carrier mobility and ultra-high thermal conductivity.^[7]


Three-dimensional graphene-based materials usually exhibit four forms that have been previously described in the literature: graphene hydrogel (GH), graphene sponge (GS), graphene aerogel (GA), and graphene foam (GF).^[8] Various methods for the preparation of graphene foam have been designed. For example, Ghorbani et al.^[9] synthesized graphene foam by a hydrothermal method, after which the discharge capacity of GF reached 321 $\text{mA}\cdot\text{h}\cdot\text{g}^{-1}$. Zhao et al.^[10] used lignin in a simple

method for the preparation of graphene foam. At a current density of 1 $\text{A}\cdot\text{g}^{-1}$, the capacitance was 183 $\text{F}\cdot\text{g}^{-1}$. Wang et al.^[11] prepared 3D-PG with chitosan as raw material, which displayed a prominent cycling durability. When graphene is doped with nitrogen, the electrochemical properties can be further improved.

Yu et al.^[12] used nitrogen-doped graphene foam as an electrode material to construct a battery and obtained, at a current density of 1 $\text{A}\cdot\text{g}^{-1}$, a discharge capacity of 180 $\text{mA}\cdot\text{h}\cdot\text{g}^{-1}$. Ping et al.^[13] prepared graphene by electrochemical exfoliation in foam nickel template with FeCl_3/HCl solution as etching agent. The maximum specific capacitance was about 128 $\text{F}\cdot\text{g}^{-1}$ at a current density of 1 $\text{A}\cdot\text{g}^{-1}$. Han et al.^[14] prepared 3D-PG by using sugar blowing-assisted thermal reduction and interconnection of graphene oxide. The 3D-PG films showed a capacitance of about 115 $\text{F}\cdot\text{g}^{-1}$ at a scan rate of 10 $\text{mV}\cdot\text{s}^{-1}$. Luo et al.^[15] prepared 3D-PG by a chemical reduction and self-assembly method in which tannic acid (TA) was used as reducing agent. Liu et al.^[16] synthesized high-quality three-dimensional glucose/graphene aerogels (G/GAs) with a high specific capacitance of 305.5 $\text{F}\cdot\text{g}^{-1}$ using a hydrothermal reduction and CO_2 activation method.

In this paper, 3D-PG was prepared with graphene oxide as raw material by combining hydrothermal reduction and chemical reduction. The influence of reduction time and amount of reducing agent on porous morphology were investigated. The electrochemical performance of 3D-PG were measured by building a three-electrode system with 3D-PG as the electrode and an aqueous KOH solution as the electrolyte.

[a] Dr. H. Liu, B. Sun, P. Zhu, C. Liu, Prof. Dr. G. Zhang, Dr. D. Wang, X. Song, Dr. J. Shi, Dr. Y. Yang, Dr. J. Lu
Beijing Institute of Graphic Communication
School of Printing and Packaging Engineering
102600 Beijing (P. R. China)
E-mail: zhanggaimei@bigc.edu.cn

 © 2022 The Authors. Published by Wiley-VCH GmbH. This is an open access article under the terms of the Creative Commons Attribution Non-Commercial License, which permits use, distribution and reproduction in any medium, provided the original work is properly cited and is not used for commercial purposes.

Experimental Section

Chemicals

Single layer GO powder with high purity was bought from Suzhou Tanfeng Graphene Technology Co., Ltd., China. Acetone and AA were bought from Shanghai Aladdin Biochemical Technology Co., Ltd., China. Nickel foam, conductive carbon black and polytetrafluoroethylene (PTFE) were purchased from Taiyuan Lizhiyuan Technology Co., Ltd., China. Absolute ethanol and potassium hydroxide were purchased from Beijing Tong Guang Fine Chemical Company, China.

Preparation of 3D graphene

60 mg of GO powder were dispersed in 30 mL of deionized water under ultrasonic conditions. Three solutions were prepared by using different amount of AA, that is, the ratios of GO to AA were 1:0, 1:1, and 1:2, respectively. The solutions were then heated to 180 °C and the reaction times were set as 4 h, 8 h, 12 h, 16 h, 20 h and 24 h, respectively. The obtained graphene hydrogel was washed several times with water, then it was refrigerated to prevent the graphene sheets from restacking, where the temperature was -70 °C. The preparation process framework of graphene hydrogel is shown in Figure 1.

The reduced graphene oxide (RGO) was denoted as R, and the prepared samples with the ratios of GO to AA as 1:0, 1:1 and 1:2 were denoted as R0, R1 and R2, respectively. The samples prepared for 4 h reaction times at the ratios of GO to AA as 1:0, 1:1 and 1:2 were written as R0-4, R1-4 and R2-4, respectively. Therefore, the reaction time of 8 h at the ratio of GO to reducing agent as 1:2, the sample was denoted as R2-8. A similar naming approach was chosen for the samples with reaction times of 12, 16, 20, 24 h, and so on.

Characterization

In order to explore the effects of reducing agent and reduction time on sample characterizations, the crystal structures and chemical bonds of GO and 3D-PG were characterized by X-ray diffraction (XRD) (Bruker, Germany D8 ADVANCE X) and Fourier-transform infrared spectroscopy (FTIR) (FTIR Nicolet IS10). The morphology of 3D-PG was observed by scanning electron microscopy (SEM) (SU8020-Hitachi SU8000 Series). The pore size and pore distribution were measured using the Brunauer–Emmett–Teller approach (BET) (APSP 2460 Series). All electrochemical measurements (cyclic voltammetry, constant charge/discharge current, cycle life performance, EIS) were carried out using an electrochemical

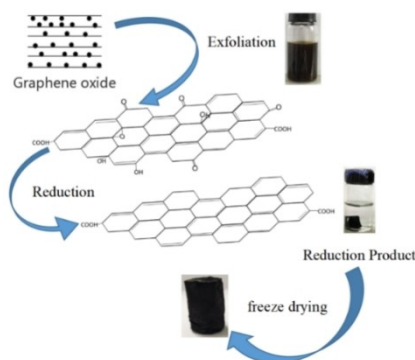


Figure 1. Schematic diagram of the preparation process for 3D-PG.

workstation (CS350 Potentiostat/Galvanostat, Wuhan Corrtest Instruments Corp Ltd., China), in which a three-electrode cell system was constructed with a 6.0 M KOH electrolyte. For the working electrode, the mixed slurry was used by mixing 3D-PG conductive carbon black and PTFE at mass ratio of 8:1:1, which was 5 mg. The mixed slurry was coated on the surface of nickel foam and was then dried.

Results and Discussions

Characterizations

FTIR

Figure 2 shows the FTIR spectrum of GO, R0 and R2 with reaction times of 4 h, 12 h and 20 h, respectively, in the range of 4000–400 cm^{-1} . There were absorption peaks at 3340, 1734, 1630 and 1410 cm^{-1} , which corresponded to O–H stretching vibration, C=O stretching vibration, C=C bending vibration, and R–OH deformation, respectively.^[8]

Compared to GO, the hydroxyl peak and oxygen-containing groups of 3D-PG samples were significantly reduced, which indicated that 3D-PG remained the original graphene structure with a low oxidation rate and a high purity. The peak intensities of hydroxyl and oxygen-containing groups were gradually reduced along with the increase of reductant dose and the reaction time. So the reaction time and amount of agent affected the degree of GO reduction.

XRD

The XRD patterns of GO, R0 and R2 prepared at reaction times of 4 h, 8 h and 12 h, respectively, are shown in Figure 3. The diffraction peak of GO appeared at about 10°, while the

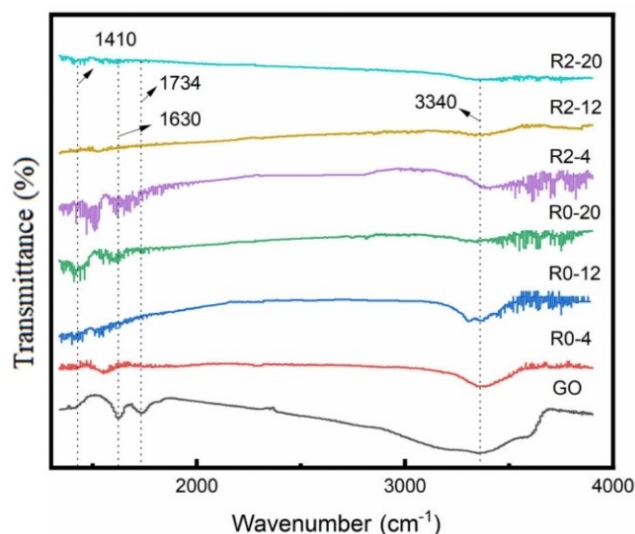


Figure 2. FTIR spectrum of GO and various 3D-PGs.

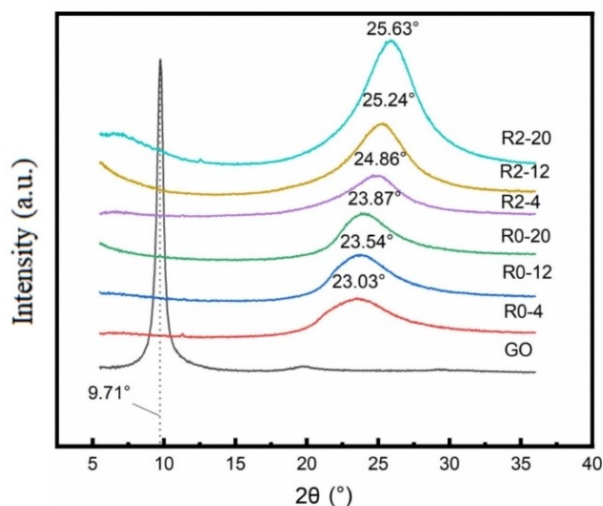


Figure 3. X-ray diffraction patterns of GO and various 3D-PGs.

diffraction peaks of 3D-PG samples were located at about 25° , and the peak intensity also decreased, which indicates the occurrence of reduction reaction of GO,^[8] removing oxygen-containing groups. The graphene layers were stacked together due to van der Waals forces, resulting in a smaller distance between the layers. Comparing the samples R0 and R2, it was found that the peak shifting caused by reductant dosage was greater than that caused by the reaction time, by which it could be deduced that the role of reductant in the structure was greater than reaction time.

Besides, it was seen that for same reaction time, the diffraction peak gradually shifted to the right with the increase of the reducing agent amount. The maximum angle appeared at R2-20, where the full width at half maxima (FWHM) was minimum, which indicated that the layer space was the

smallest. Using the Scherrer Equation, the calculated layer space was 0.35 nm.

The Layer spacing can be calculated by Equation (1)

$$2d\sin\theta = n\lambda \quad (1)$$

Where d is the interplanar spacing, θ is the diffraction angle, λ ($\lambda = 0.154$ nm) represents the wavelength of X-ray and n ($n = 1$) is the diffraction order.

SEM

The morphology of 3D-PGs in different amounts of reductant was investigated by scanning electron microscope (SEM). Figures 4 to 6 show the morphologies of three samples prepared at different dosages of reducing agent and different reaction times.

Figure 4 shows the images of sample prepared with different ratios of GO to reducing agent and the reducing time of 20 h. Figure 5 shows the images of sample prepared without reducing agent in pure hydrothermal process, while Figure 6 is the images of R2 samples with different reducing time. By comparing, it could be seen that the accumulation at the edge area around the hole increased along with the reaction time, resulting in a slight decrease of the pore size.

It showed that the pore diameter of the samples prepared at ratio of GO to reducing agent as 1:1 (R1) and 1:2 (R2) were larger and more uniform than that prepared by pure hydrothermal (R0). The pore sizes in R0, R1 and R2 were in the ranges of 0.5–1 μm , 1–1.5 μm , and 1.5–3 μm , respectively. Compared with the three-dimensional graphene formed by the pure hydrothermal method, the pore distribution of the samples with reducing agent was more uniform and the pore diameter was much larger. The results showed that the combination of large specific surface area and uniform pore size distribution could improve the electrochemical performance, which was

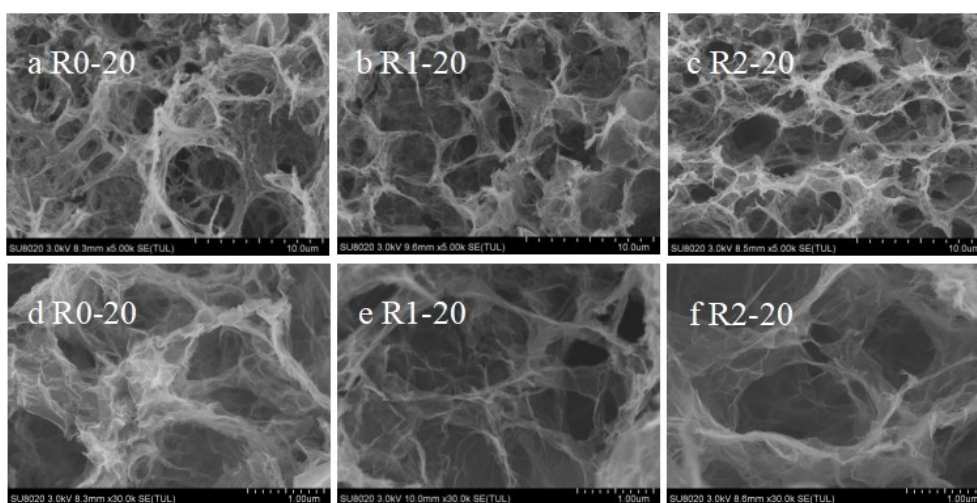


Figure 4. SEM images of 3D-PG prepared with different ratios of GO to reducing agent ((a) R0, (b) R1 and (c) R2 at magnification of 5 K, while (d) R0, (e) R1 and (f) R2 at magnification of 30 K).

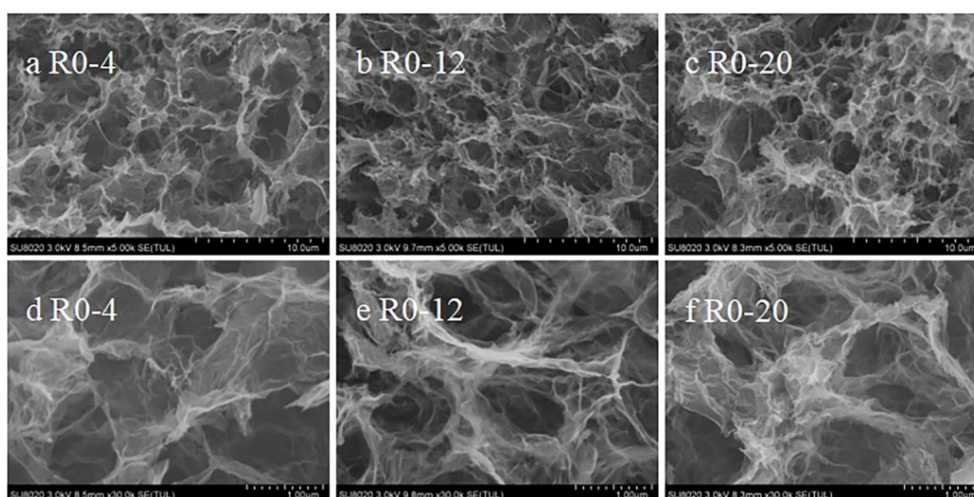


Figure 5. SEM images of 3D-PG prepared with different reduction times and without reducing agent ((a) R0-4, (b) R0-12, and (c) R0-20 at magnification of 5 K; (d) R0-4, (e) R0-12, and (f) R0-20 at magnification of 30 K).

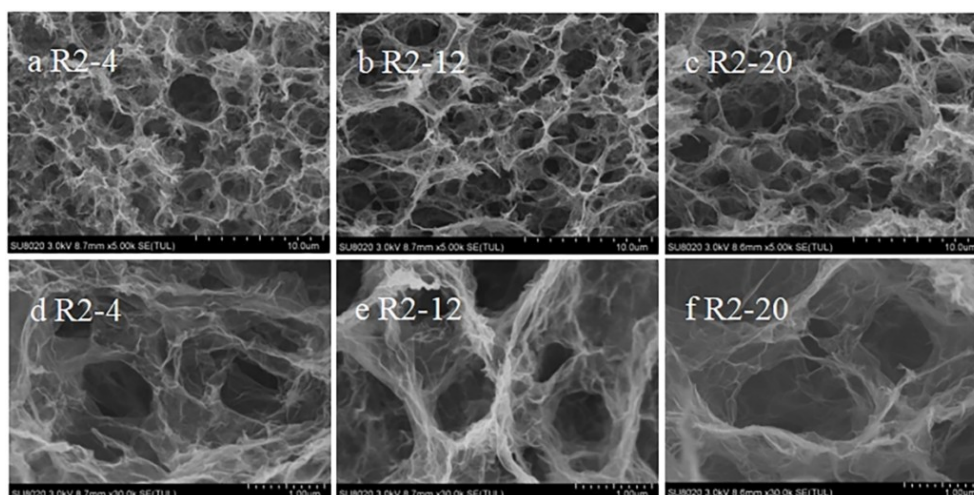


Figure 6. SEM images of 3D-PG prepared with ratio of GO/reducing agent as 1:2 and different reduction times ((a) R2-4, (b) R2-12, and (c) R2-20 at magnification of 5 K; (d), (e), and (f) at magnification of 30 K).

consistent with previous results.^[17] It could be concluded that the reducing agent played an important role in pore size.

BET

The micropore distributions were investigated by BET for samples R0-20 and R2-20 prepared using different reductant dosages, and samples of R2-4, R2-12 and R2-20 with different reaction times, respectively.

The micropore distribution of samples are shown in Figure 7 and Figure 8. Figure 7 is the micropore distributions of R0-20 and R2-20 with different reductant dosages. It could be seen that for R0-20 most pore diameters were below 1 nm, whereas for R2-20 the diameters of all pores were above 1 nm. With the increase of reductant dosage, the aggregation increased and

the layer space decreased. The number of micropores with small pore size decreased gradually.

Comparing R2-4 and R2-12 prepared with different reducing times, it results that more micropores below 1 nm in diameter were in R2-4, while more micropores above 1 nm in diameter were in R2-12. Therefore, it can be concluded that increasing the reducing time will cause much more the aggregation of GO, the decrease of layer space, and the decrease of small pore size micropore population.

The number of micropores and the connectivity of micropores greatly affect the electrochemical performance.^[18] Han et al.^[19] prepared graded porous graphene aerogels by template assisted freeze casting and thermal reduction, which can adjust the porosity of micropores to increase the thermal stability and specific surface area of graphene aerogels. In this paper, VC hydrothermal reduction of graphene oxide powder was used to adjust the amount of reducing agent and the reduction time to

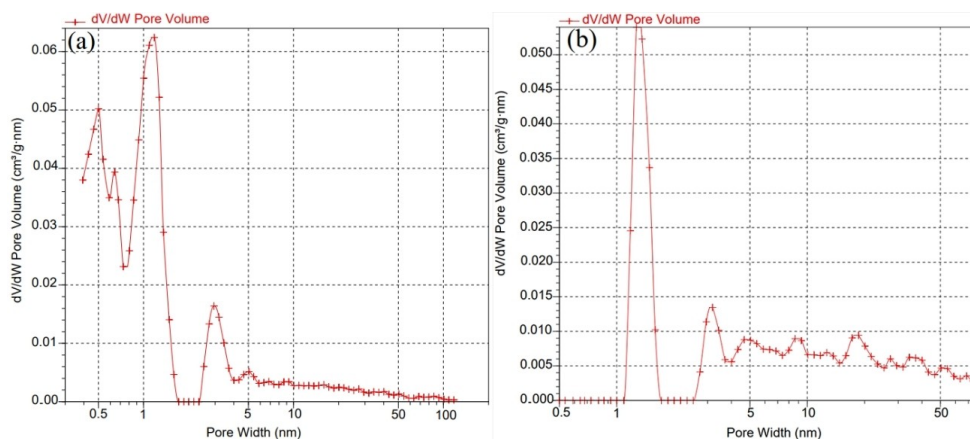


Figure 7. BET test curve for 3D-PG of (a) R0-20, (b) R-20.

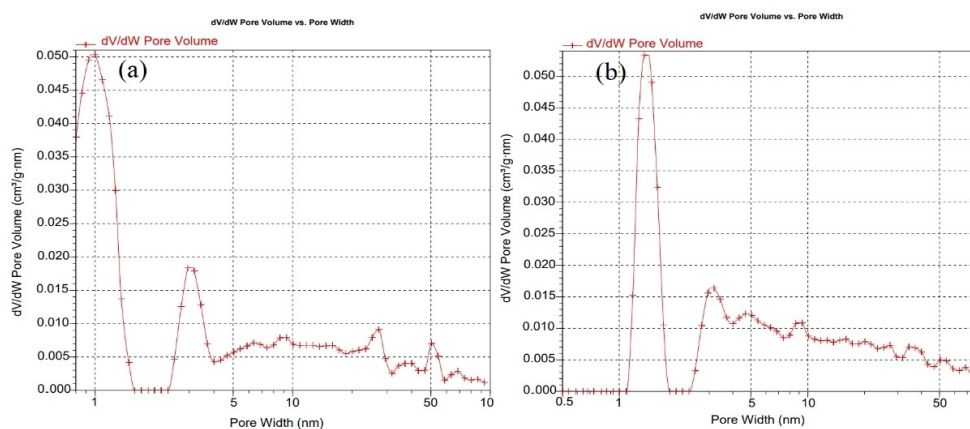


Figure 8. BET test curve for 3D-PG of (a) R2-4, (b) R2-12.

adjust the number of micropores, so as to adjust the connectivity of 3D-PG pores to enhance the electrochemical performance of materials.

Table 1 shows the specific surface area, single point adsorption pore capacity and average adsorption pore diameter. When the mass ratios of GO to AA are 1:0 and 1:2, the average pore sizes are 6.37 nm and 12.74 nm, respectively. When the reactive times are 4 h, 12 h and 20 h, the average pore sizes and the specific surface areas are 10.97 nm, 12.54 nm, 12.74 nm and $180.57 \text{ m}^2 \cdot \text{g}^{-1}$, $189.91 \text{ m}^2 \cdot \text{g}^{-1}$, $192.41 \text{ m}^2 \cdot \text{g}^{-1}$, respectively. It was found that the average pore size and volume increase along with the amount of reductants.

Sample	Specific Surface Area [$\text{m}^2 \cdot \text{g}^{-1}$]	Single Point Adsorption Pore Capacity [$\text{cm}^3 \cdot \text{g}^{-1}$]	Average Adsorption Pore Diameter [nm]
R0-20	225.27	0.36	6.37
R2-4	180.57	0.50	10.96
R2-12	189.91	0.59	12.55
R2-20	192.41	0.60	12.74

Electrochemical Properties

Cyclic voltammetry (CV)

All electrochemical measurements were conducted in a three-electrode system at room temperature using a 6 M solution of KOH as the electrolyte. The Pt and Ag/AgCl electrodes were used as the counter electrode and the reference electrode, respectively.

Figure 9 shows the CV plots of 3D-PG constructed electrode. It can be seen that the closed cyclic voltammetry presents a quasi-rectangular shape, no appearance of redox peaks from Faraday reactions, indicating that the sample has good electric double-layer capacitance characteristics.^[20] For the $50 \text{ mV} \cdot \text{s}^{-1}$ scanning rate, in general, the area of closed CV increased at the beginning and then decreased with the increase of reaction time. The capacitance characteristics were the best in the samples prepared at the 12 h and 20 h reaction times.

In Figure 10, it was found that the for sample prepared with reaction time of 12 h the area of CV decreased along with the increase of the proportion of reducing agent, while for sample prepared with reaction time of 20 h, it increased initially and then decreased. It was noticed that the area of CV in R0 and R1

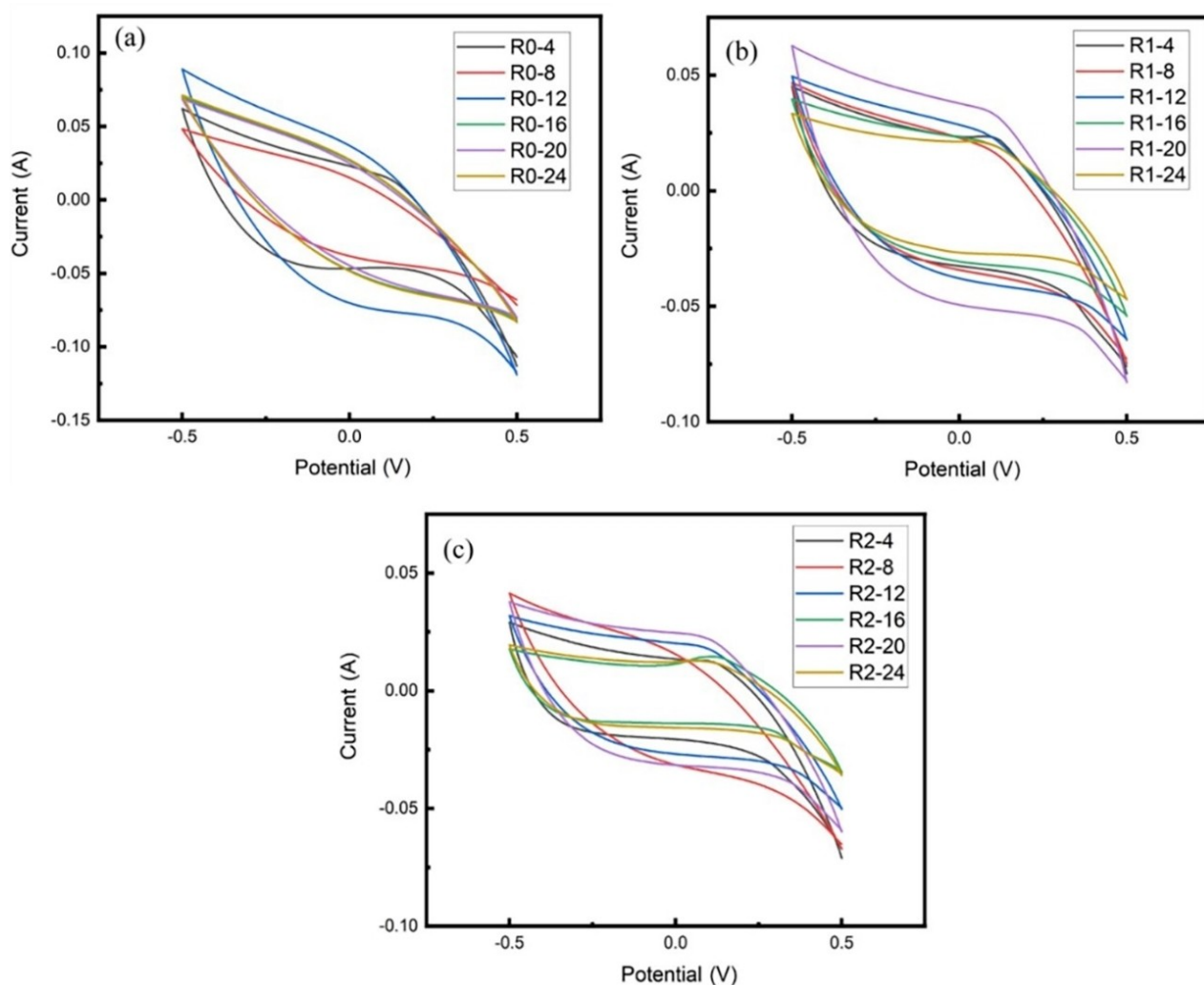


Figure 9. CV plots of (a) R0, (b) R1, (c) R2 samples prepared with different reaction times.

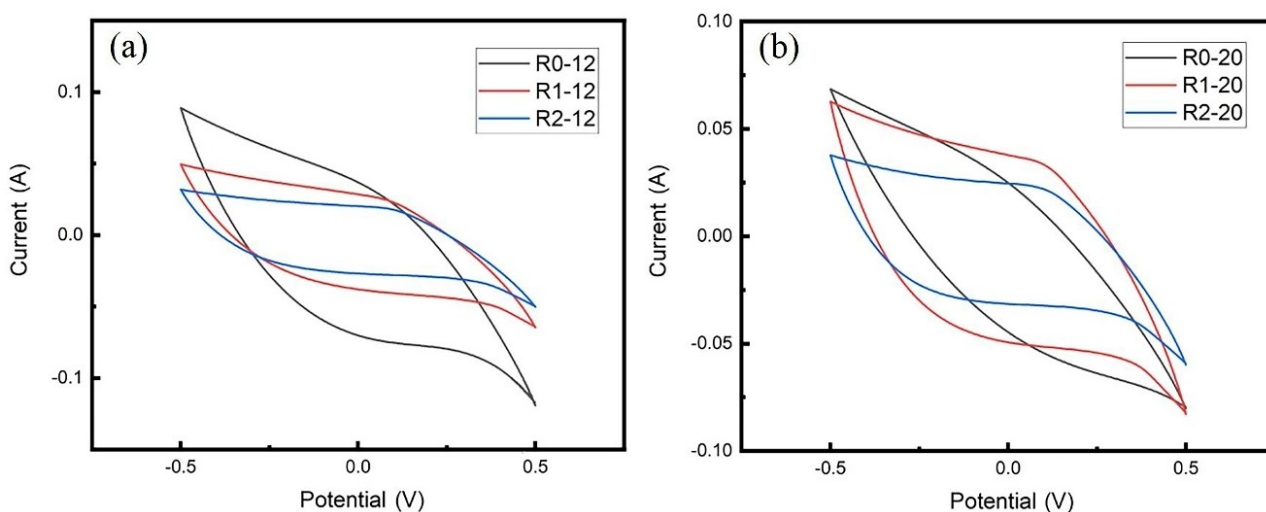


Figure 10. CV of R0, R1 and R2 samples with reaction times of (a) 12 and (b) 20 h.

was larger than that in R2, which indicated that the specific capacitance of R0 and R1 was higher. The porous structure of 3D-PG has a short charge transfer distance, so it will provide an excellent charge transfer path in the issue of charge/discharge process.^[21] When the reaction time was 20 h, the area of the sample R1-20 was the largest (see Figure 10b). It was clear that in the case of long reaction time, the reducing agent increased the number of pores in 3D-PG, which provided a good charge transfer path. Figure 11(a) and Figure 11(b) present the CV of samples R0-12 and R1-20 at 5, 10, 20, 50 and 100 mV·s⁻¹ scanning rates, respectively. Among them, the CV area of R0-12 and R1-20 was the largest at the rate of 100 mV·s⁻¹ and 50 mV·s⁻¹ respectively.

The specific capacitance can be calculated by Equation (2):

$$C = \frac{1}{s \cdot m \cdot \Delta V} \int_{V_0}^{V_0+\Delta V} i dV \quad (2)$$

Where s is the scanning rate (V·s⁻¹), m is the mass (g), v is the potential (V), and i is the current (A).

Then CV area of R1-20 at 100 mV was 0.06, and the specific capacitances was 153.5 F·g⁻¹. It was achieved that R1-20 existed a better electrochemical performance. Compared to specific capacitance of 169 F·g⁻¹ measured for material obtained by the low-temperature liquid phase method,^[22] our data was comparable, meanwhile the process was facile, safe, and environmentally friendly. Compared with the 115 F·g⁻¹ determined by sugar blowing-assisted reduction and interconnection of graphene oxide into three-dimensional porous graphene,^[21] the results showed that our method was comparative.

Electrochemical impedance measurement

Electrochemical impedance spectroscopy (EIS), as an important electrochemical characterization, is mainly used to evaluate impedance and capacitive behavior. Figure 12 shows the

electrochemical impedance spectra of R0, R1 and R2 in the frequency range from 0.01 Hz to 100 kHz by applying an AC voltage with a disturbance of 5 mV, and the equivalent circuit was fitted with Zview. The circuit was composed of two resistors, one capacitor and one Warburg impedance (Figure 12(d)). The relevant resistance of R1-20 was 4.307 Ω. It was found that it followed the typical supercapacitor AC impedance spectrum with a high, intermediate and low frequency areas. In the low frequency region, the electrochemical impedance was an approximate vertical line, indicating the resistance generated by the diffusion and transmission of electrolyte ions on the surface of 3D-PG was small, deducing a better double-layer capacitance behavior.^[23] It was noticed that for the same reaction time, the electrochemical performance of 3D-PG electrode increased initially and then decreased with the increase of reductant dosage. For the same reductant dosage, the electrochemical performance also increased initially and then decreased along with the reaction time. This indicated that with the increase of reductant dosage and reaction time, the stack of reduced graphene oxide increased, the specific surface area was relatively small, leading to the reduction of electrochemical properties. According to CV and constant current charge/discharge curves, the capacitance effect of R1-20 was the best.

Conclusions

In summary, the influence of reaction time and the amount of reducing agent in 3D-PG fabrication on the properties were investigated. It was found that the reduction of 3D-PG gradually increased, and the electrochemical performance of the prepared electrode by using the 3D-PG samples was improved along with the reaction time and the ratio of GO to reducing agent. But with a long reaction time or a large ratio of reducing agent, the 3D-PG would stack and the layer space decreased, which caused the decrease of specific surface area and the

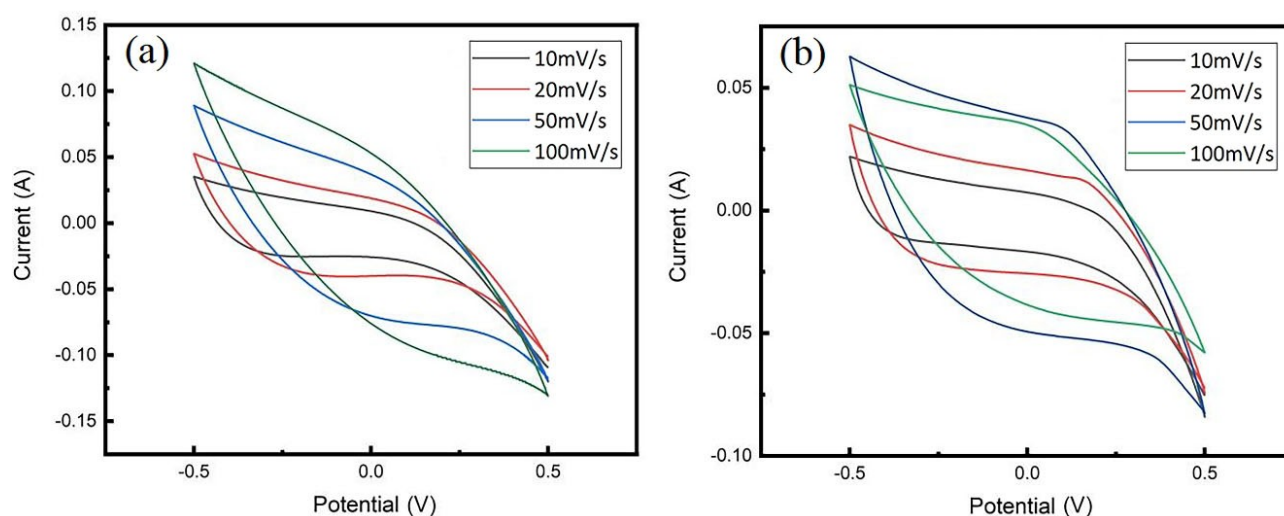


Figure 11. CV of R0 and R1 samples at different scanning rates.

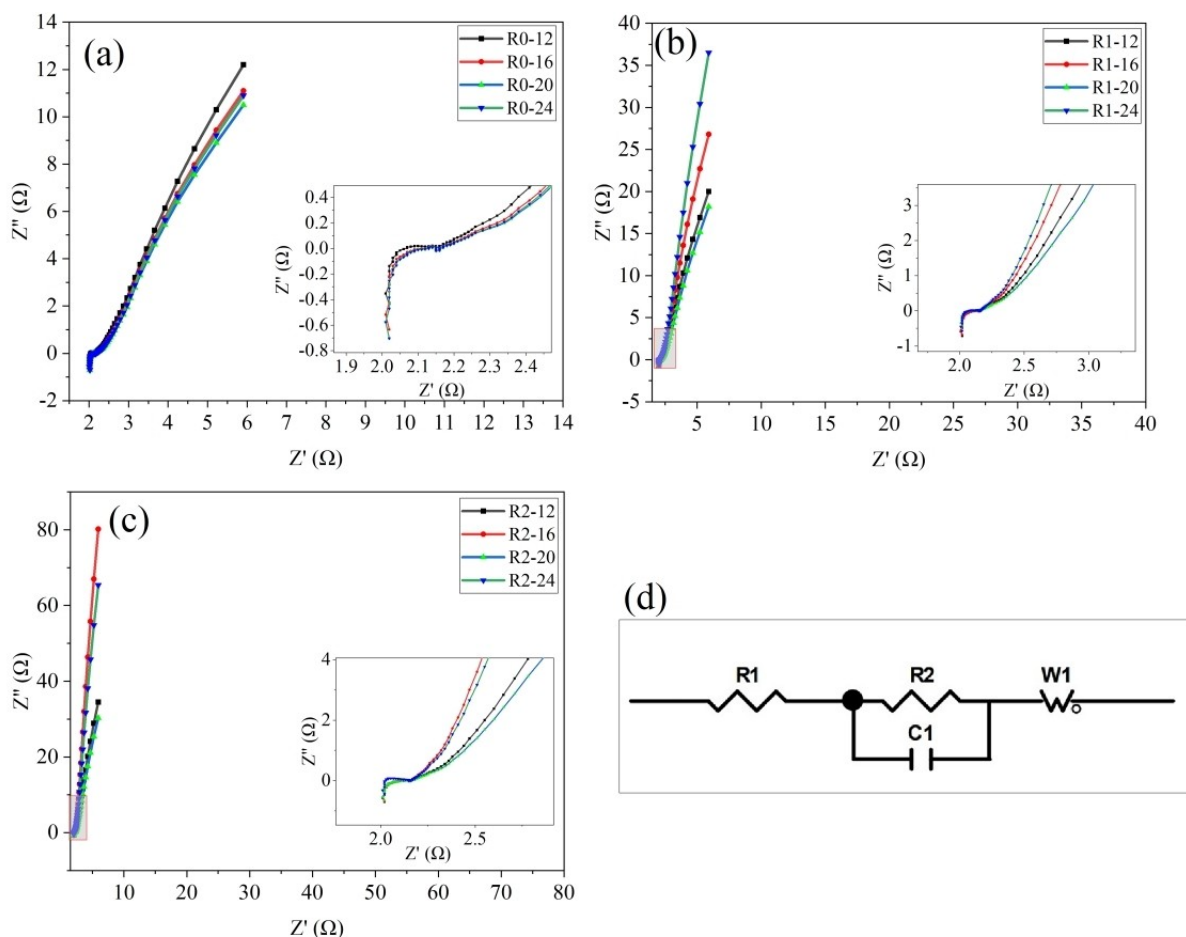


Figure 12. The electrochemical impedance spectra of (a) R0, (b) R1, (c) R2, (d) Zview equivalent circuit diagram.

electrochemical performance. In the optimal condition, the maximum specific capacitance is $153.5 \text{ F} \cdot \text{g}^{-1}$, the according material thus being expected to be useful as electrode material in supercapacitors.

Acknowledgement

This work was supported by the National Natural Science Foundation of China (No. 51305038); Key Research Project of Beijing Institute of Graphic Communication (No Ed202104, Eb202201) and Doctoral initiation fund project of Beijing Institute of Graphic Communication (No. 27170122011).

Conflict of Interest

The authors declare no conflict of interest.

Data Availability Statement

Research data are not shared.

Keywords: 3D porous graphene · electrochemistry · hydrothermal reduction · specific capacitance · specific surface area

- [1] a) X. Du, I. Skachko, A. Barker, E. Y. Andrei, *Nat. Nanotechnol.* **2008**, *3*, 491–495; b) K. I. Bolotin, K. J. Sikes, Z. Jiang, M. Klima, G. Fudenberg, J. Hone, P. Kim, H. L. Stormer, *Solid State Commun.* **2008**, *146*, 351–355.
- [2] X. Zhang, K. S. Ziemer, B. L. Weeks, *Adv. Compos. Hybrid. Mater.* **2019**, *2*, 492–500.
- [3] a) P. T. Xu, J. X. Yang, K. S. Wang, Z. Zhou, P. W. Shen, *Chin. Sci. Bull.* **2012**, *57*, 2948–2955; b) F. Li, J. Qu, Y. Li, J. H. Wang, *Adv. Sci.* **2020**, *7*, 2001561; c) K. Li, H. Teng, X. J. D-ai, Y. Wang, D. S. Wang, X. F. Zhang, Y. J. Yao, X. Y. Liu, L. Feng, J. S. Rao, Y. X. Zhang, *CrystEngComm* **2002**, *24*, 2081–2088.
- [4] a) Z. S. Wu, D. W. Wang, W. Ren, J. P. Zhao, G. M. Zhou, F. Li, H. M. Chen, *Adv. Funct. Mater.* **2010**, *20*, 3595–3602; b) Y. F. Ma, Y. S. Chen, *Natl. Sci. Rev.* **2015**, *2*, 40–53.
- [5] C. Li, G. Q. Shi, *Nanoscale* **2012**, *4*, 5549–5563.
- [6] B. L. Sun, J. Y. Cai, D. Li, X. D. Gou, Y. Q. Gou, W. Li, F. D. Hu, *Chinese. J. Anal. Chem.* **2019**, *47*, 271–279.
- [7] a) S. J. Guo, S. J. Dong, *Chem. Soc. Rev.* **2011**, *40*, 2644–2672; b) K. Leng, F. Zhang, L. Zhang, T. F. Zhang, Y. P. Wu, Y. H. Lu, Y. Huang, Y. S. Chen, *Nano Res.* **2013**, *6*, 581–592; c) Y. J. Chen, J. Zhu, B. H. Qu, B. A. Lu, Z. Xu, *Nano Energy* **2014**, *3*, 88–94; d) J. Zhu, Z. H. Zhang, X. Z. Yu, Q. H. Li, B. A. Lu, Z. Xu, *Nano Energy* **2014**, *3*, 80–87; e) J. Zhu, D. N. Lei, G. H. Zhang, Q. H. Li, B. G. Lu, T. H. Wang, *Nanoscale* **2013**, *5*, 5499–5505.
- [8] L. Z. Guan, L. Zhao, Y. J. Wan, L. C. Tang, *Nanoscale* **2018**, *10*, 14788–14811.

- [9] R. Ghorbani, S. Behrangi, H. Aghajani, A. T. Tabrizi, N. Abdian, *Mater. Sci. Eng. B* **2021**, *268*, 115139.
- [10] Y. Zhao, M. Y. Wen, C. H. He, C. L. Liu, Z. R. Li, Y. Liu, *Mater. Lett.* **2020**, *247*, 30752–30758.
- [11] C. Wang, G. B. Zhong, W. Zhao, S. J. Wu, W. Su, Z. F. Wei, K. Q. Xu, *Front. Energy Res.* **2020**, *8*, 00061.
- [12] H. Yu, D. L. Ye, T. Butburee, L. Z. Wang, M. Dargusch, *ACS Appl. Mater. Interfaces* **2016**, *8*, 2505–2510.
- [13] Y. J. Ping, Y. N. Gong, Q. Fu, C. X. Pan, *Prog. Nat. Sci.* **2017**, *27*, 177–181.
- [14] F. M. Han, O. Qian, B. Chen, H. B. Tang, M. L. Wang, *J. Alloys Compd.* **2018**, *730*, 386–391.
- [15] J. Luo, J. P. Lai, N. Zhang, Y. B. Liu, R. Liu, X. Y. Liu, *ACS Sustainable Chem. Eng.* **2016**, *4*, 1404–1413.
- [16] S. Sun, X. F. Ma, *NANO* **2016**, *11*, 64–72.
- [17] X. Y. Luo, S. R. Chen, T. Z. Hu, Y. Chen, F. Li, *SusMat* **2021**, *1*, 211–240.
- [18] a) C. N. Wang, L. J. Bai, F. Zhao, L. Z. Bai, *Carbon Lett.* **2022**, *32*, 907–915; b) L. L. Sun, Z. B. Zhao, Y. Sun, X. Z. Wang, X. G. Liu, Y. Z. Yang, J. S. Qiu, *Diamond Relat. Mater.* **2020**, *106*, 107827.
- [19] Q. Han, L. Yang, Q. L. Liang, M. Y. Ding, *Carbon* **2017**, *122*, 556–563.
- [20] a) M. Kazazi, M. Faryabi, *J. Power Sources* **2020**, *449*, 227510; b) C. Phrompet, K. Maneesai, W. Tuichai, A. Karaphun, C. Sriwong, *J. Energy Storage* **2020**, *30*, 101474.
- [21] S. M. Sun, S. Wang, T. C. Xia, X. F. Li, Q. X. Jin, Q. Wu, L. Z. Wang, Z. H. Wei, P. Y. Wang, *J. Mater. Chem. A* **2015**, *3*, 20944–20951.
- [22] L. N. Xu, M. Q. Wang, L. Li, Z. Yang, J. J. Li, *Mater. Res. Express* **2019**, *6*, 055603.
- [23] Y. N. Gong, D. L. Li, Q. Fu, C. X. Pan, *Prog. Nat. Sci.* **2015**, *25*, 379–385.

Manuscript received: August 13, 2022

Revised manuscript received: September 28, 2022
